

Modeling of Drying Process in Porous Media

AHMET AYDIN¹, CHARLÉLIE BILODEAU², CHARLOTTE BECKFORD³,
GAOHUI ZHANG⁴, HANIYEH FATTAHPOUR⁵, IRENE ERAZO⁶, OLAYEMI ADEYEMI⁷,
PER WAGENIUS⁸, PK KATABOH⁹, HANGJIE JI*

¹ *University of Maryland, Baltimore County, Baltimore, MD, USA.*

² *Polytechnique Montréal, Montréal, QC, Canada.*

³ *University of Tennessee, Knoxville, TN, USA.*

⁴ *University of Minnesota-Twin Cities, MN, USA.*

⁵ *Georgia State University, Atlanta, Georgia, USA.*

⁶ *Tulane University of Louisiana, New Orleans, LA, USA.*

⁷ *Boise State University, Boise, ID, USA.*

⁸ *University of Vermont, Burlington, VT, USA.*

⁹ *University of Delaware, Newark, DE, USA.*

* *Mentor - North Carolina State University Raleigh, NC, USA.*

Study Group: 18th Annual Graduate Student Mathematical Modeling Camp, University of Delaware, June 7 – 11, 2023.

Key Words: Partial differential equations, free boundary problems, fluid dynamics, reaction-diffusion models, filtration, evaporation, particle deposition, porous media, and heat flux.

Summary

Mathematical modeling of drying in porous media is a valuable tool for understanding and optimizing the drying process. During the GSMMC camp, we explored two approaches to modeling the drying process: microscopic and macroscopic. In the microscopic model, the focus is on the individual pores and their interactions. This approach considers the movement of moisture at a microscale level, accounting for factors such as pore size, shape, and connectivity. It involves complex calculations and is suitable for detailed analysis of specific porous structures. The microscopic model provides insights into the internal dynamics of drying, such as capillary effects and local moisture distribution. On the other hand, the macroscopic model takes a more simplified approach by considering the porous material as a homogenous medium. It describes the overall behavior of the drying process at a larger scale, treating the absorbent material as a continuum. The macroscopic model employs equations that represent the average properties of the material, such as moderate moisture content and temperature. This approach is computationally less intensive and provides a broader understanding of the drying process. Both the microscopic and macroscopic models have their advantages and limitations. The microscopic model offers detailed insights into the intricate mechanisms occurring at the pore level but requires extensive computational resources. The macroscopic model simplifies the drying process but cannot capture local variations and specific pore-level interactions.

1 Introduction

The drying process in porous media is a complex phenomenon in various industrial, environmental, and biological applications. A porous material's physical, chemical, and mechanical characteristics are drastically altered when moisture is extracted from the empty spaces inside the material. Mathematical modeling of the drying process in porous media provides a powerful tool for understanding the underlying physics and optimizing drying operations. Modeling drying processes in porous media requires a multidisciplinary approach combining fluid mechanics, heat transfer, mass transfer, and material science principles. The goal is to develop mathematical equations that describe the transport mechanisms involved in moisture removal and predict the distribution of moisture content, temperature, and other relevant variables within the porous structure as a function of time and position.

Commonly, fundamental conservation rules, including mass, momentum, and energy conservation, are used to create mathematical models for drying in porous media. These laws are applied to the porous medium, accounting for fluid flow and heat and mass transfer within the material. The models consider various transport mechanisms, including diffusion, convection, and capillary action, which play a crucial role in drying. Mass transfer in drying occurs primarily through diffusion, where moisture moves from regions of high concentration to areas of low concentration within the porous material. Fick's law of distribution is commonly used to describe moisture transport, considering factors such as concentration gradients, porosity, and tortuosity of the porous media. Additionally, convective mass transfer can occur due to gas or liquid flow through the porous structure, influencing the drying rate.

Energy transfer during drying is also a vital aspect to consider. Heat transmission mechanisms such as conduction, convection, and radiation influence the rate of evaporation and drying. The energy equation incorporates temperature gradients and considers heat fluxes between the porous material, the surrounding environment, and applied heat sources. Heat transfer modeling is essential for understanding the interplay between moisture removal and energy consumption in the drying process. The porous structure itself plays a significant role in the drying process. The absorbent material's geometry, porosity, and pore size distribution affect its permeability, capillary effects, and transport properties. The modeling of drying in porous media often requires characterizing these properties and considering how they influence the drying behavior. Mathematical modeling of drying processes in porous media enables a deeper understanding of the fundamental mechanisms involved and provides valuable insights for process optimization. By accurately predicting drying rates, moisture profiles, and energy requirements, these models can aid in the design of efficient drying operations, reduce energy consumption, and optimize product quality [1].

Furthermore, computational techniques and numerical simulations have become indispensable for modeling drying processes. Complex mathematical models may be solved using sophisticated numerical methods, including finite element analysis, finite difference approaches, and computational fluid dynamics. These techniques can offer extensive information regarding temperature and moisture distribution inside porous structures. In recent years, the development of mathematical models has been facilitated by computer

hardware and software advancements. High-performance computing enables the solution of complex and computationally intensive models, providing detailed predictions of drying behavior in porous media. These models can account for various complexities, such as non-linearities, phase changes, and multi-physics phenomena, thereby enhancing the accuracy of predictions. The drying modeling in porous media applies to various industries and processes. For example, understanding agricultural products' drying behavior in food processing can improve preservation methods, reduce waste, and enhance product quality. In construction, modeling the drying of concrete and other building materials can help optimize curing times and prevent structural issues. In environmental engineering, the drying of soils and sediments plays a role in groundwater management and land reclamation projects [2].

The drying process exhibits a multi-scale nature, which both the microscopic and macroscopic models can capture. In the macroscopic model, the entire porous medium is considered as a whole rather than focusing on individual pores. The variables such as average moisture content (\hat{y}), average temperature (\hat{T}), and length scale (\hat{L}) are used to describe the overall behavior of the drying process. The macroscopic model provides an overview of the drying process and is represented by equations such as $(\hat{y}) = hT((\hat{x}), (\hat{t}))$ and $(\hat{y}) = hB((\hat{x}), (\hat{t}))$, where hT and hB represent the moisture content at the top and bottom of the porous medium, respectively. The macroscopic model encompasses evaporation in the wet region ($\hat{\Omega}_w$) and a dry region ($\hat{\Omega}_d$), where the drying process occurs.

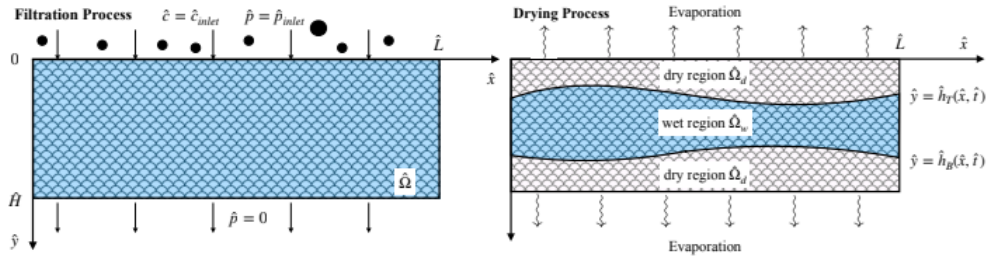


Figure 1. Macroscopic model (reproduced from [3])

On the other hand, the microscopic model considers the deposition of particles and liquid evaporation at the pore scale. It focuses on the interactions between individual pores and captures the intricacies of particle deposition and liquid evaporation phenomena. The microscopic model provides detailed insights into the mechanisms occurring at the pore level, including filtration processes. It involves variables such as inlet pressure (\hat{p}_{inlet}) and inlet concentration (\hat{c}_{inlet}) to represent particle deposition and liquid evaporation processes.

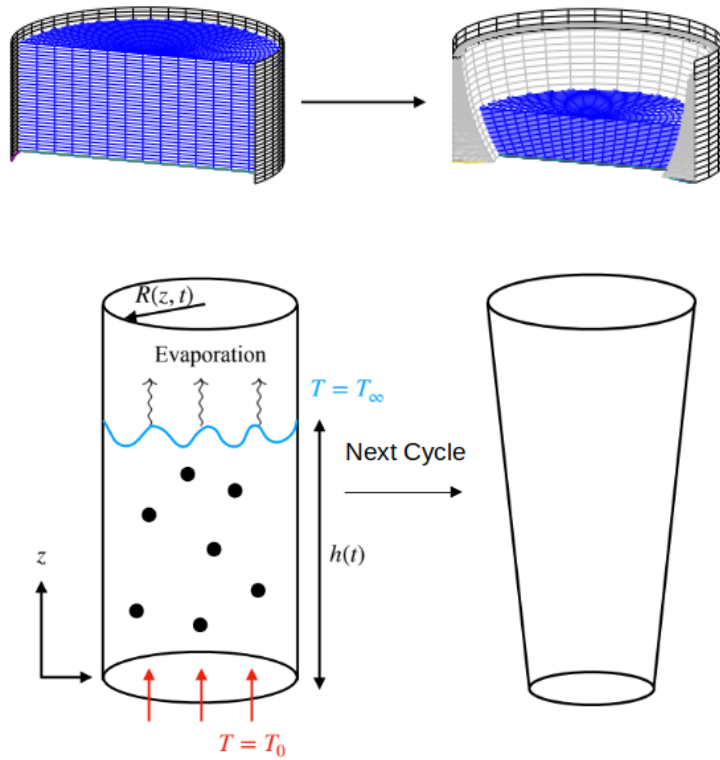


Figure 2. Microscopic model. The top panel is reproduced from [4].

Both the macroscopic and microscopic models contribute to understanding the drying process. The macroscopic model provides a broader view and simplifies the analysis, while the microscopic model offers detailed information about pore-level interactions and phenomena. By combining these models, a comprehensive understanding of the multi-scale nature of the drying process can be achieved.

Mathematical modeling of the drying process in porous media is a multidisciplinary endeavor that combines principles from fluid mechanics, heat transfer, mass transfer, and material science. It provides a systematic approach to understanding the complex physical and transport phenomena occurring during drying. By accurately predicting drying rates, moisture distribution, and energy requirements, these models offer insights for optimizing drying operations in various industrial, environmental, and biological applications. The advancement of computational techniques has further enhanced the accuracy and applicability of these models, contributing to improved processes and product quality in diverse fields.

2 Microscopic Model

The heat equation

$$\frac{\partial T}{\partial t} = \kappa \nabla^2 T \quad (2.1)$$

describes the time and spatial evolution of temperature T , with κ being a constant. At equilibrium,

$$\frac{\partial T}{\partial t} = 0, \quad (2.2)$$

so that, using cylindrical coordinates, (2.1) becomes

$$\frac{1}{r} \frac{\partial}{\partial r} \left(r \frac{\partial T}{\partial r} \right) + \frac{\partial^2 T}{\partial z^2} = 0. \quad (2.3)$$

Let H and R be scaling factors associated with the height of the liquid and the pore's radius respectively. Defining \hat{z} and \hat{r} , such that [4]

$$z = H\hat{z}, \quad 0 \leq \hat{z} \leq 1, \quad (2.4)$$

$$r = R\hat{r}, \quad 0 \leq \hat{r} \leq 1, \quad (2.5)$$

equation (2.3) can be written as

$$\left(\frac{H}{R} \right)^2 \frac{1}{\hat{r}} \frac{\partial}{\partial \hat{r}} \left(\hat{r} \frac{\partial T}{\partial \hat{r}} \right) = - \frac{\partial^2 T}{\partial \hat{z}^2}. \quad (2.6)$$

Assuming that $H \ll R$, the left-hand side of (2.6) vanishes, which leads to

$$T(z, t) = A(t)z + B(t), \quad (2.7)$$

where $A(t)$ and $B(t)$ are constant with respect to z that need to be determined and that have absorbed the constant coming from the change of variable performed in (2.4). The boundary conditions needed to get a particular solution of temperature $T(t, z)$ come from the conservation of energy at the interface between the liquid and the atmosphere, that is the evaporation rate E is

$$E = - \left. \frac{\partial T}{\partial \mathbf{n}} \right|_{z=h} = - \left. \frac{\partial T}{\partial z} \right|_{z=h}, \quad t \geq 0 \quad (2.8)$$

at the interface, which is considered to be flat and of height $h = h(t)$. Its normal vector is $\mathbf{n} = \hat{\mathbf{z}}$, the unit vector pointing in the z direction. Moreover, the evaporation rate must verify

$$k_0 E = k_1 (P - P_v) + (T(h, t) - T_\infty), \quad t \geq 0 \quad (2.9)$$

where k_0 and k_1 are constants, P is the pressure of the atmosphere at the interface with the liquid, P_v is the liquid's vapor pressure, T_∞ is the temperature of the atmosphere, far from the liquid. Additionally, since the bottom of the pore is kept at a constant temperature T_0 from a heat source,

$$T(0, t) = T_0, \quad t \geq 0. \quad (2.10)$$

Inserting boundary conditions (2.8)–(2.10) into (2.7) yields

$$T(z, t) = -Ez + T_0, \quad (2.11)$$

where

$$E = E(h) = \frac{T_0 - T_\infty}{k_0 + h(t)}. \quad (2.12)$$

The drying of a single pore verifies

$$\begin{cases} \frac{\partial R}{\partial t} = -\chi Q(C), & 0 < z < h(t) \\ \frac{dh}{dt} = -E(h) \\ \frac{\partial}{\partial t}(CR^2) = D \frac{\partial}{\partial z} \left(R^2 \frac{\partial C}{\partial z} \right) - 2RQ(C), & 0 < z < h(t) \end{cases} \quad (2.13)$$

with boundary conditions

$$\begin{cases} D \frac{\partial C}{\partial z} \Big|_{z=0} = 0 \\ D \frac{\partial C}{\partial z} \Big|_{z=h} = EC \end{cases} \quad (2.14)$$

for $t > 0$ and where χ and D are constants, $R = R(z)$ is the radius of the pore at height z and $C = C(z, t)$ is the concentration of particles in the liquid. It is assumed that it is independent on the radial distance from the central axis of the pore. The flux Q of particles being adsorbed on the walls of the pore is proportional to the concentration exceeding the saturation concentration C_{sat} , that is

$$Q(C) = (C - C_{\text{sat}})_+, \quad (2.15)$$

where $(\cdot)_+ \equiv \max(\cdot, 0)$.

The moving upper boundary $z = h(t)$ in (2.13) can be fixed by introducing the change of variables

$$y \equiv \frac{z}{h(t)} \quad (2.16)$$

which is such that $0 < y < 1$. However, in this case, the quantities of interest R and C must be transformed by introducing \hat{R} and \hat{C} .

$$R(z, t) = \hat{R}(y, \tau) \quad C(z, t) = \hat{C}(y, \tau) \quad (2.17)$$

Performing the chain rule and change of variable, (2.13) and (2.14) change to

$$\begin{cases} \frac{\partial \hat{R}}{\partial t} - \frac{y}{h} \frac{dh}{dt} \frac{\partial \hat{R}}{\partial y} = -\chi Q(\hat{C}), & 0 < y < 1 \end{cases} \quad (2.18)$$

$$\frac{dh}{dt} = \frac{T_\infty - T_0}{k_0 + h(t)}, \quad (2.19)$$

$$\begin{cases} \frac{\partial \hat{R}^2 \hat{C}}{\partial t} - \frac{y}{h} \frac{dh}{dt} \frac{\partial \hat{R}^2 \hat{C}}{\partial y} = \frac{D}{h^2} \frac{\partial}{\partial y} \left(\hat{R}^2 \frac{\partial \hat{C}}{\partial y} \right) - 2\hat{R}Q(\hat{C}), & 0 < y < 1 \end{cases} \quad (2.20)$$

$$\begin{cases} \left[\frac{D}{h} \frac{\partial \hat{C}}{\partial y} + \frac{dh}{dt} \hat{C} \right] \Big|_{y=1} = 0 \end{cases} \quad (2.21)$$

$$\begin{cases} \frac{\partial \hat{C}}{\partial y} \Big|_{y=0} = 0 \end{cases} \quad (2.22)$$

with $t > 0$.

3 Numerical Study of the Microscopic Model

Discretization of the system of equations (2.18)–(2.22) is performed using forward differences for time derivatives and central differences for spatial derivatives. Timesteps of duration Δt and spatial steps of length $\Delta y = 1/M$ are constants. $M + 1$ is the number of grid points uniformly distributed over the y axis and is chosen sufficiently large compared to the number of timesteps so that the Courant–Friedrichs–Lewy condition is verified. Since Δt is chosen arbitrarily, the maximum of timesteps is chosen so that $h(t) > 0$ for all t . Let t_* be the time associated with the last timestep such that $h(t_*) > 0$. From (2.19), the analytical solution for h can be derived using simple variable separation, which leads to

$$t_* = \frac{1 + 2k_0}{2(T_0 - T_\infty)} \quad (3.1)$$

The discretized values of a given variable X are noted X_j^n , with the n superscript representing the timestep index and the j subscript, the grid point index. Then, (2.19) becomes

$$\frac{h^{n+1} - h^n}{\Delta t} = -\frac{T_0 - T_\infty}{k_0 + h^n} \quad (3.2)$$

which can be first solved iteratively for h^{n+1} given the initial height $h^0 = 1$. Equations (2.18) and (2.20) are discretized as

$$\begin{cases} \frac{\hat{R}_j^{n+1} - \hat{R}_j^n}{\Delta t} + \frac{j}{h^n} \frac{T_0 - T_\infty}{k_0 + h^n} \frac{\hat{R}_j^n - \hat{R}_{j-1}^n}{\Delta y} = -\chi Q(\hat{C}_j^n), & j = 1, 2, \dots, M, \\ \frac{\hat{R}_j^{n+1} - \hat{R}_j^n}{\Delta t} = -\chi Q(\hat{C}_j^n), & j = 0. \end{cases} \quad (3.3)$$

$$\begin{aligned} & \frac{\hat{C}_j^{n+1} (\hat{R}_j^{n+1})^2 - \hat{C}_j^n (R_j^n)^2}{\Delta t} + \frac{j}{h^n} \frac{T_0 - T_\infty}{k_0 + h^n} \frac{\hat{C}_{j+1}^n (\hat{R}_{j+1}^n)^2 - \hat{C}_{j-1}^n (\hat{R}_{j-1}^n)^2}{2} \\ &= \frac{D}{(h^n)^2 \Delta y} \left(\frac{(\hat{R}_{j+1}^n + \hat{R}_j^n)^2}{4} \frac{\hat{C}_{j+1}^n - \hat{C}_j^n}{\Delta y} - \frac{(\hat{R}_j^n + \hat{R}_{j-1}^n)^2}{4} \frac{\hat{C}_j^n - \hat{C}_{j-1}^n}{\Delta y} \right) \\ & \quad - 2\hat{R}_j^n Q(\hat{C}_j^n) \quad j = 1, 2, \dots, M - 1 \end{aligned} \quad (3.4)$$

The boundary conditions (2.21) and (2.22) become

$$\frac{D}{h^{n+1}} \frac{3\hat{C}_M^{n+1} - 4\hat{C}_{M-1}^{n+1} + \hat{C}_{M-2}^{n+1}}{2\Delta y} = \frac{T_0 - T_\infty}{k_0 + h^n} \hat{C}_M^{n+1} \quad (3.5)$$

and

$$\frac{-3\hat{C}_0^{n+1} + 4\hat{C}_1^{n+1} - \hat{C}_2^{n+1}}{2\Delta y} = 0. \quad (3.6)$$

respectively.

Given initial concentration $\{\hat{C}_j^0\}_{j=0}^M$ and radius $\{\hat{R}_j^0\}_{j=0}^M$, $\{\hat{R}_j^1\}_{j=0}^M$ can be determined using (3.3). Using these values, $\{\hat{C}_j^1\}_{j=1}^{M-1}$ is obtained using (3.4). The missing \hat{C}_0^1 and \hat{C}_M^1 can then be calculated with (3.5) and (3.6). This process is repeated for all subsequent timesteps, until $t = t_*$. Two sets of parameters are considered for the numerical examples, see table 1. In the first simulations initial radius considered to be uniform

Parameter description	Symbol	Cylindrical pore	Non-uniform case
Timestep	Δt	$2.5 \cdot 10^{-3}$	10^{-4}
Number of spatial gridpoints	M	20	20
Volume scaling coefficient	χ	0.8	1
Precipitation rate coefficient	λ	1	0.7
Saturation concentration	C_{sat}	0.4	0.25
Initial concentration	C_0	$0.5 + 0.1 \sin(\pi y)$	$0.4 - 0.1z$
Diffusion coefficient	D	0.1	1
Initial radius	R_0	1	$0.1 + 0.05 \sin(3\pi z)$
Source temperature	T_0	1.2	1.3
Environment temperature	T_∞	1	1
Evaporation coefficient	k_0	1	0.2

Table 1. Numerical values of parameters appearing in system of equations (3.2)–(3.6)

with respect to z , i.e. case of cylindrical pore. The solution is over-saturated with a sinusoidal distribution of particles. The simulation results are shown in figure 3; as a result of the small change in evaporation rate over time the height of the fluid decreases almost linearly, the concentration at different timesteps in function of the normalized spatial coordinate y is constant in space with small increase at the fluid interface, and uniformly decreases with each time-step. Similarly, radius of the pore decreases linearly over time. Courant–Friedrichs–Lewy (CFL) condition imposes small Δt relative to Δy . Therefore, to limit computational requirements the simulations are done over short period of time.

As shown in Fig. 4, we present a series of snapshots that provide insight into the behavior of the channel during the drying process. As indicated in the figure, this row represents a particular time point, which represents the evolution of the channel between $t = 0.01$, $t = 0.51$ and $t = 0.91$. From these snapshots, it is evident that the pore interface has changed over time. As an example, in Fig. 4(b), we can see a snapshot of the pore at a particular time ($t = 0.51$). It has been observed that the radius of the pore and the concentration of solute decrease along the length of the pore. There is no expansion of the channel, rather it continues to shrink until it reaches a steady state. During the course of time, the three-dimensional representation of the pore changes, showing alterations throughout its length. The change in shape is the result of several factors, including a shrinking radius, a decrease in pore concentration, an increase in temperature, and a decrease in pore height (3).

Figure 5 illustrates snapshots of the pore’s cross-section from a top view, illustrating how its radius changes with time (t). During the drying process, these snapshots provide a visual representation of how the pore radius changes over time. We can observe in the figures the temporal variation in the pore radius, which sheds light on its dynamic behavior. As a result of these insights, it is possible to gain a better understanding of the drying process and its effects on pore structure. As a result of such data, drying operations can be optimized, energy efficiency can be improved, and product quality can be improved in a variety of industries and applications.

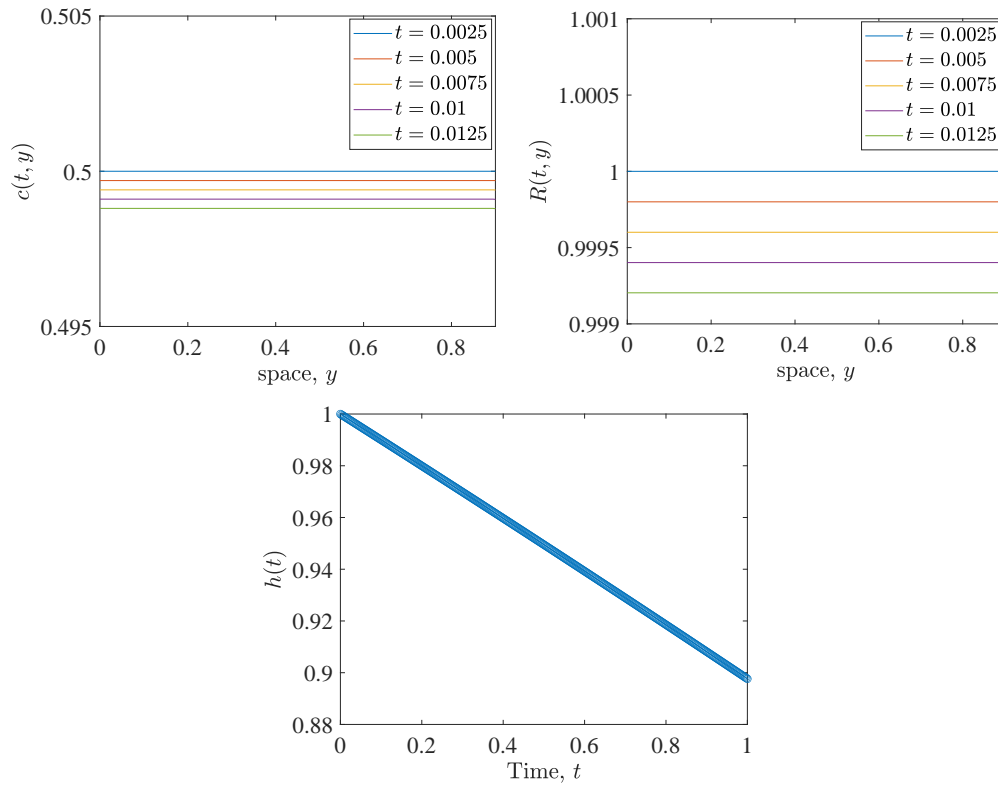


Figure 3. Plot of concentration C , radius R in space over 400 time steps and height $h(t)$, respectively, with the parameter $k_0 = 1, T_0 = 1.2, T_\infty = 1, \chi = 0.8, D = 0.1$, and final time is $t_f = 1$.

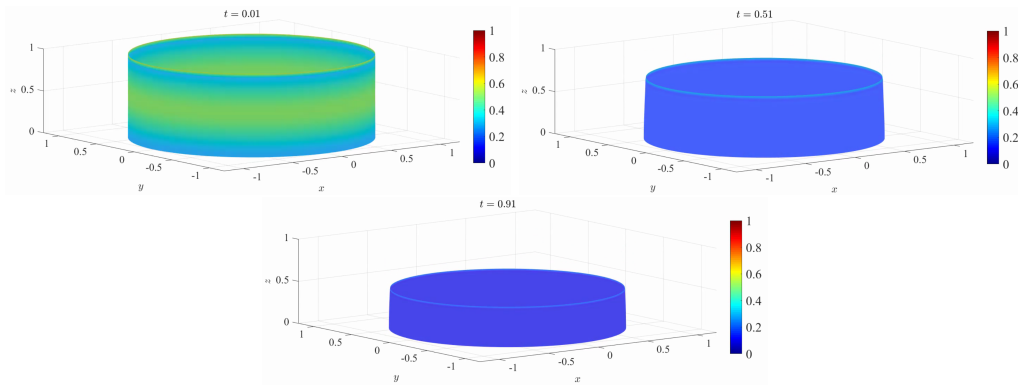


Figure 4. Changing the channel. Snapshots of the pore at $t = 0.01, t = 0.51$ and $t = 0.91$ are shown in (a)-(c), for the parameters $k_0 = 1, T_0 = 1.2, T_\infty = 1, \chi = 0.8, D = 0.1$, $C_0 = 0.5 + 0.1 * \sin(\pi * y)$ and final time is $t_f = 1$. The color-bar shows the concentration. For a clear visualization, see Video.mov as a Supplementary Information (SI).

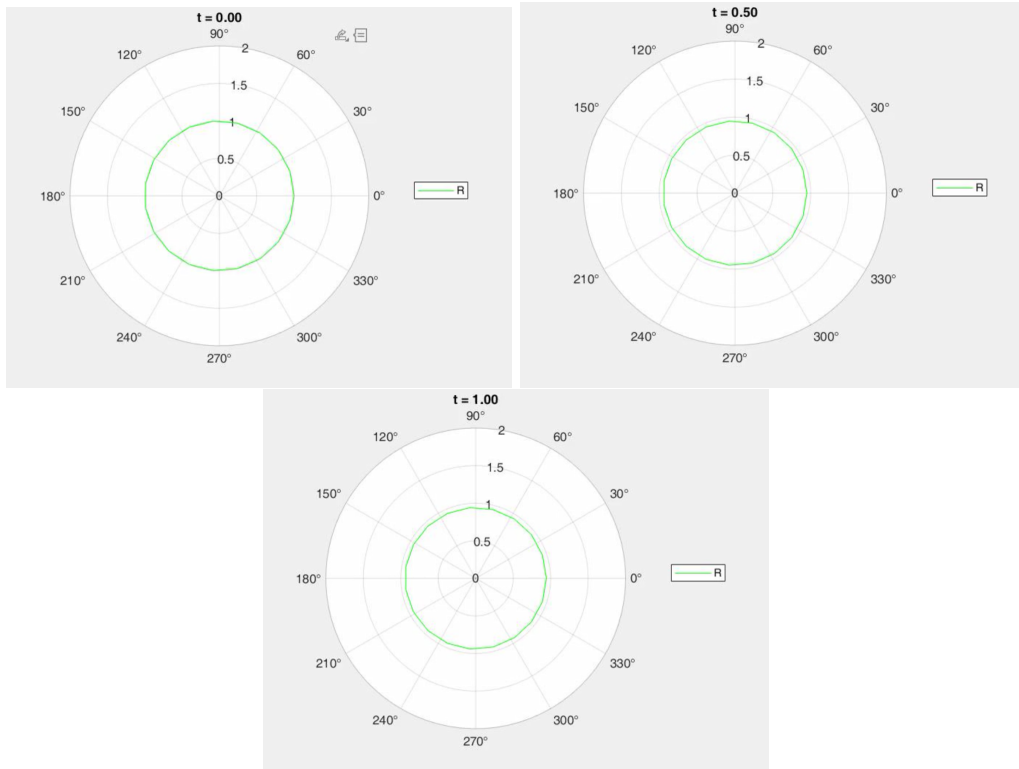


Figure 5. Snapshots of the radius at $t = 0$, $t = 0.5$ and $t = 1$ are shown in (a)-(c), for the parameters $k_0 = 1$, $T_0 = 1.2$, $T_\infty = 1$, $\chi = 0.8$, $D = 0.1$, and final time is $t_f = 1$. The color-bar shows the concentration. For a clear visualization, see simulation-video.mov as a Supplementary Information (SI).

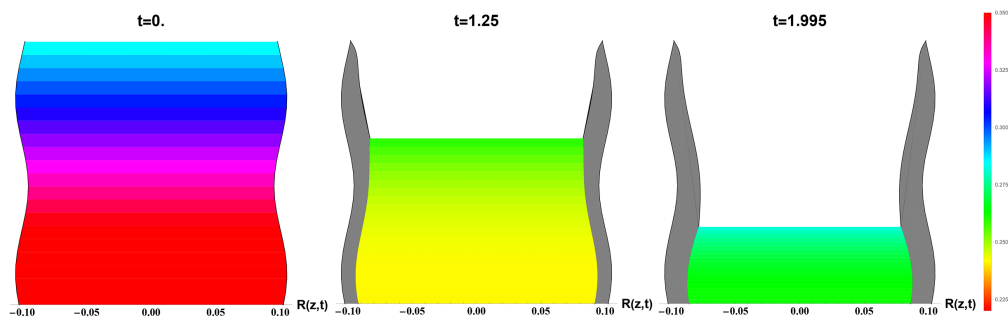


Figure 6. Overall shape of the pore with the solution given for $t \approx 0, 1.25, 2$ where the parameters chosen are given in Table 1 non-uniform case columns. The color bar show the concentration of particles, $C(z, t)$, in the solution.

In the second simulation, the pore is considered to have a non-uniform initial shape. Since the solution is oversaturated initially, particles get absorbed into the walls of the pore. This causes an overall reduction in the concentration. Then as the fluid is evaporated at the interface, the concentration increases starting at the interface. In Figure 6 the evaluation of the pore is shown for three different time frames, where the color bar indicates the concentration of particles. The same behavior is clearly observed in Figure 7a where oversaturated concentration decreases initially then starts to increase due to high evaporation rate and the radius of the pore decreases in particular on the interface, see Figure 7b.

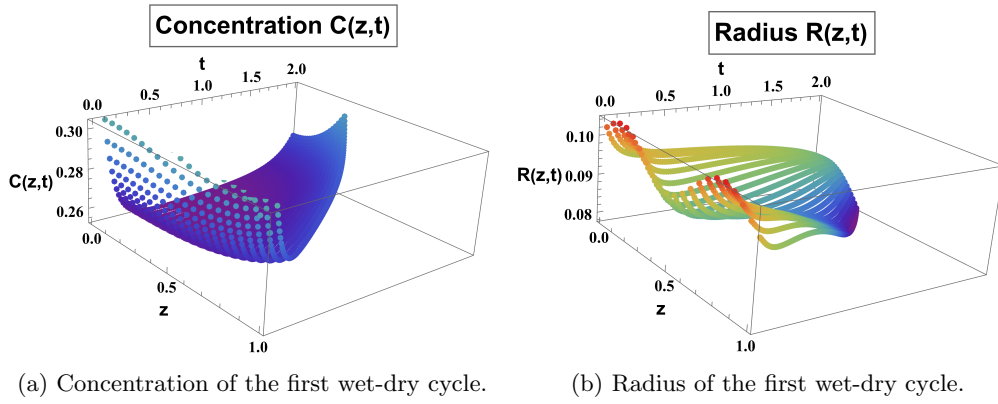


Figure 7. Concentration and radius of the pore during the first wetting-drying cycle where parameters are chosen as in Table 1 non-uniform case.

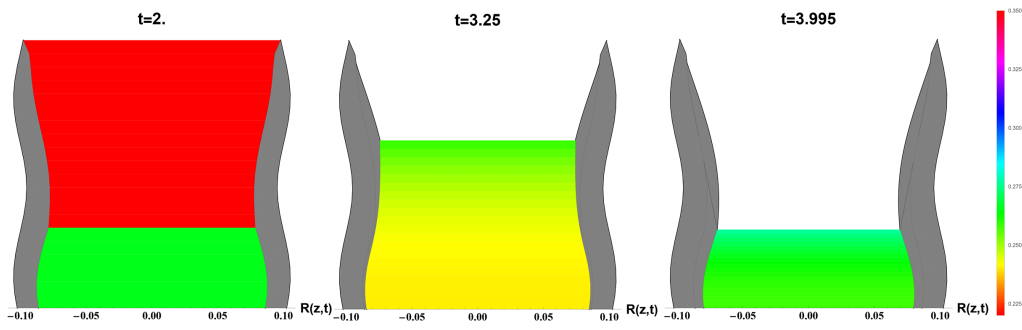
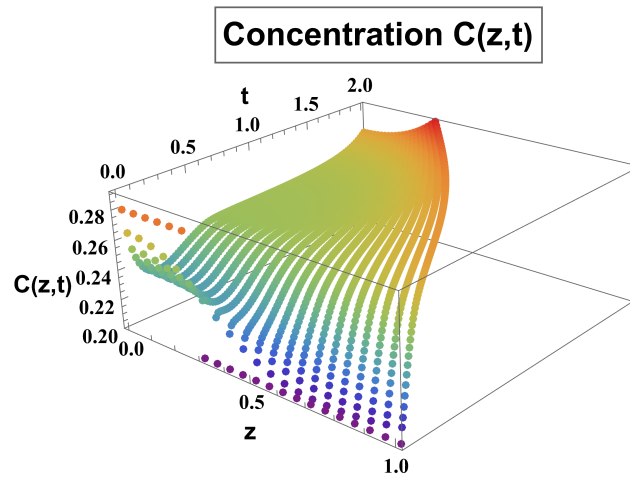
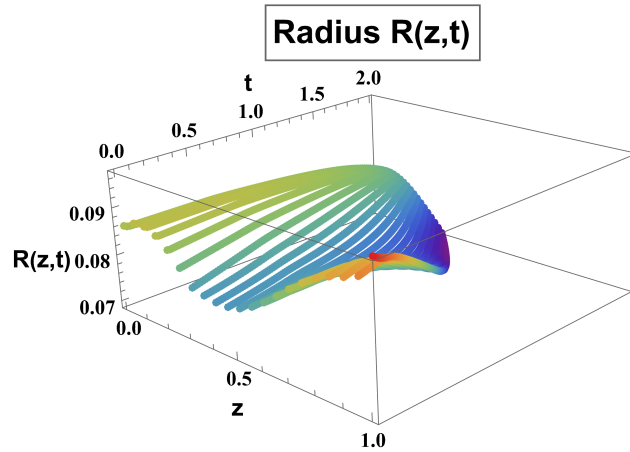


Figure 8. After the first cycle the pore is filled with a diluted solution of 0.2 concentration. The overall shape of the pore with the solution given for $t \approx 2, 3.25, 4$ where the parameters were chosen as the final state of the first cycle with added fluid. The color bar shows the concentration of particles, $C(z, t)$, in the solution.



(a) Concentration of the second wet-dry cycle.



(b) Radius of the second wet-dry cycle.

Figure 9. Concentration and radius of the pore during the second wetting-drying cycle where the initial state is chosen to be as the final state of the first cycle with the addition of diluted solution.

After the first cycle the pore is filled with a diluted solution of 0.2 concentration and a second drying cycle is considered, see Figure 8. This time due to a lower concentration of particles initial decrease in the radius is not observed. However, due to evaporation the concentration increases and the radius decreases at the boundary, see Figure 9.

Observe that the concentration rate increases beyond the saturation levels even in the undersaturated conditions, see Figure 9a. In some of the simulations, the "blowing-up" of the concentration levels is observed. This can be seen to be the result of a high evaporation rate where the adsorption of particles into pore walls is not sufficiently fast to compensate for the loss of fluid. This discrepancy can be fixed by considering the effect of change in radius and concentration at the interface.

4 Macroscopic Model

In this section, we extend to the multiple-pore structure or continuum model. We extend the findings from the pore-scale model to more complex scenarios. This includes considering a multiple-pore structure or developing a macroscopic continuum model. The results broaden our understanding of the drying process, considering the interactions and collective behavior of multiple pores or the overall media structure. This extension contributes to the development of more efficient and optimized drying techniques and improves our ability to predict the structure and performance of porous media after the drying process.

We start by looking at two cases: First, we assume that the evaporation is negligible. We consider

$$\frac{dh}{dt} = -E \quad (4.1)$$

$$k_o E = k_1(P - P_v) + T - T_\infty \quad (4.2)$$

We start assuming that h does not move, which implies

$$\frac{dT}{dt} = 0$$

On the other hand we also assume $k_1 = 0$, that is,

$$k_o E = T - T_\infty \quad (4.3)$$

Using the above assumption and the heat equation $\frac{dT}{dt} = \alpha^2 \nabla^2 T$, we get

$$\nabla^2 T = 0.$$

Since $T(z, t) = T_0$ and $T(z, t) = T_\infty$ the solution for T is given by

$$T = T_0 + \frac{(T_\infty - T_0)z}{h}.$$

We are interested in having h dependent on time. However, if we consider

$$T = T_0 + \frac{(T_\infty - T_0)z}{h(t)}, \quad (4.4)$$

we have $dT/dt \neq 0$, contradicting one of our assumptions.

Next, we assume that the temperature is quasi-static, with

$$\frac{dT}{dt} \approx 0.$$

Obtaining from equation (4.4)

$$\frac{(T_\infty - T_0)z}{h^2} \frac{dh}{dt} \approx 0,$$

which implies from the evaporation equation (4.6)

$$E \approx 0.$$

Now, using equation (4.3) $T(h) \approx T_\infty$, then we have

$$T_o \approx T_\infty.$$

On the other hand, to work numerically we introduce the change of variables

$$y = \frac{z}{h(t)}$$

so that the computational domain becomes $y \in [0, 1]$. From the heat equation

$$\frac{dT}{dt} = \alpha^2 \frac{d^2T}{dz^2}$$

and using chain rule we get

$$\frac{dT}{dt} - \frac{y}{h} \frac{dh}{dt} \frac{dT}{dy} = \frac{\alpha^2}{h^2} \frac{d^2T}{dy^2} \quad (4.5)$$

with the domain fixed on $[0, 1]$. If $z = h$ we get $y = 1$ then from equation (4.3)

$$\frac{dh}{dt} = -E = \frac{T_\infty - T(1, t)}{k_0} \quad (4.6)$$

where $T(1, t)$ is the interface temperature. We have the boundary conditions

$$\begin{cases} T(0, t) = T_0, & t \geq 0 \\ \frac{\partial T}{\partial y} = \frac{(T_\infty - T(1, t))}{k_0} h(t), & y = 1. \end{cases} \quad (4.7)$$

To numerically solve the system of equations (4.5)-(4.6), we employ the forward Euler method on time and centered spatial discretization. We mesh the domain ($y \in [0, 1]$), where y_0, y_1, \dots, y_N represent discrete points on the grid.

From equations (4.5) and (4.6) with boundary conditions we have the following numerical scheme

$$\frac{h^{j+1} - h^j}{\Delta\tau} = \frac{T_N^j - T_\infty}{k_0} \quad (4.8)$$

$$\frac{T_i^{j+1} - T_i^j}{\Delta\tau} - \frac{i}{h^{j+1}} \frac{h^{j+1} - h^j}{\Delta\tau} \frac{T_{i+1}^j - T_{i-1}^j}{2} = \frac{\alpha^2}{(\Delta y h^{j+1})^2} \frac{T_{i-1}^j - 2T_i^j + T_{i+1}^j}{(\Delta y)^2} \quad (4.9)$$

In figure 10 (a), we present the temperature at different y values over time changing. In figure 10 (b), we illustrate the temperature and the moving boundary $h(t)$, we can appreciate how the liquid height h is decreasing when we heat the bottom, with an initial value of 1.0. We shrink the temperature along y by times $h(t)$.

After implementing our PDE code, we changed our parameter values T_0 , α , and k_0 to visualize how these parameters affect the evaporation. We show the results of some of these experiments in Figures 11 - 13. Figure 11 displays how changing these parameter values affects the evaporation rate, or the decrease of the height $h(t)$ of the evaporation boundary over time. Figure 12 displays how changing these parameter values affects the increase of the temperature of the evaporation boundary over time. Figure 13 displays how changing these parameter values affects the temperature profile throughout the solution at a single time step.

The second scenario we consider here is more general, where we assume that the evaporation is not negligible. We set the temperature as a linear equation on z , i.e

$$T(z) = T_o + bZ,$$

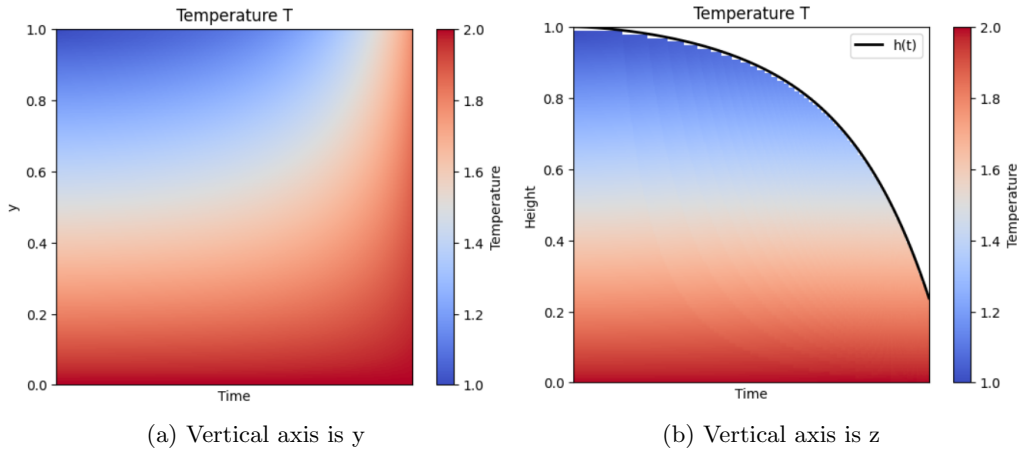


Figure 10. Plot of temperature T and height $h(t)$ in space over 400 time steps with the parameter $k_0 = 1, T_0 = 2, T_\infty = 1, \alpha = 1, \Delta y = 0.01, \Delta t = 0.00001$.

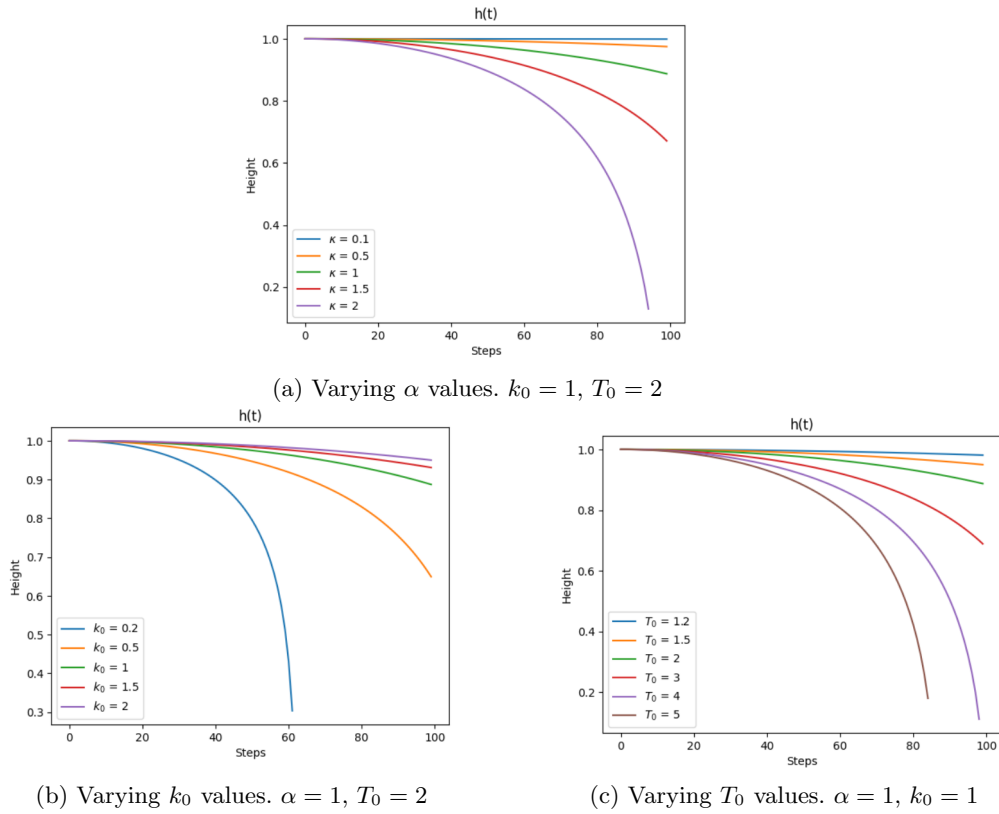
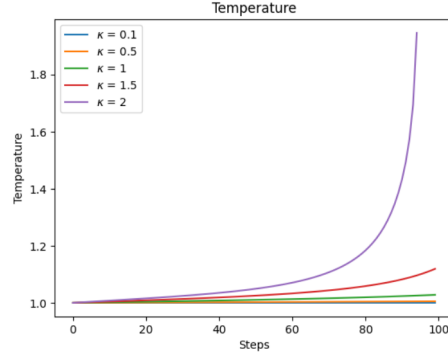
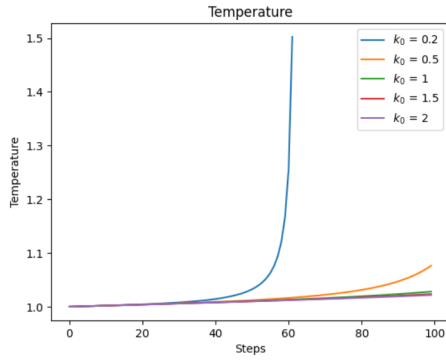
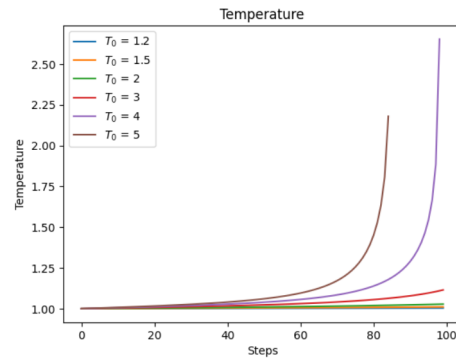


Figure 11. Plot of height $h(t)$ of interface over 100 time steps with common parameters $T_\infty = 1, \Delta y = 0.1, \Delta t = 0.00001$.

(a) Varying α values. $k_0 = 1$, $T_0 = 2$ (b) Varying k_0 values. $\alpha = 1$, $T_0 = 2$ (c) Varying T_0 values. $\alpha = 1$, $k_0 = 1$ Figure 12. Plot of temperature of interface over 100 time steps with common parameters $T_\infty = 1$, $\Delta y = 0.1$, $\Delta t = 0.00001$.

with boundary conditions

$$\begin{cases} k_o E = T - T_\infty, & z = h \\ E = -\frac{\partial T}{\partial z}, & z = h \end{cases} \quad (4.10)$$

then we have

$$\frac{dT}{dz} = b = -E,$$

which leads to

$$T(Z) = T_o - Ez.$$

If $z = h$, then

$$T(h) = T_o - Eh = T_o - \frac{(T(h) - T_\infty)h}{k_o}.$$

Denoting $T(h) = T_I$ as the interface temperature, we have

$$k_o T_I = K_o T_o - (T_I - T_\infty)h$$

$$T_I = \frac{k_o T_o + T_\infty h}{k_o + h}.$$

Note that if $T_o = T_\infty$, we get $T_I = T_o$, so the interface temperature is the same. Besides,

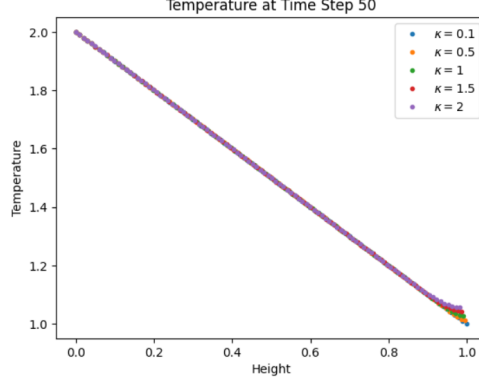
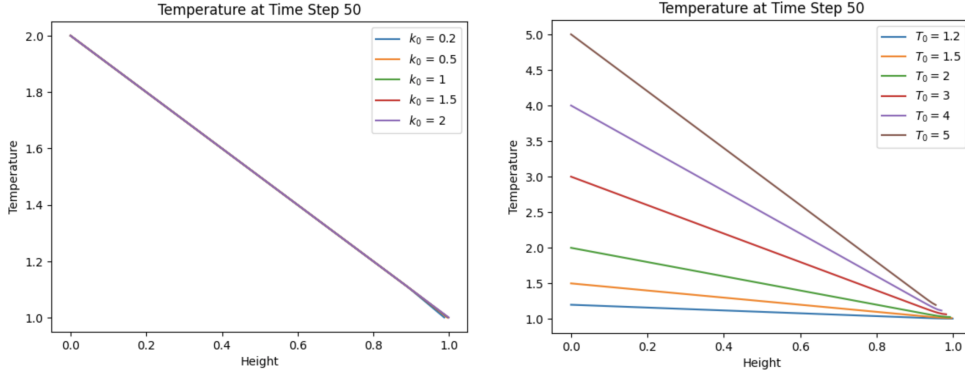
(a) Varying α values. $T_0 = 2$, $k_0 = 1$, $\Delta y = 0.01$ (b) Varying k_0 values. $\alpha = 1$, $T_0 = 2$, $\Delta y = 0.1$ (c) Varying T_0 values. $\alpha = 1$, $k_0 = 1$, $\Delta y = 0.01$

Figure 13. Plot of the temperature profile of the solution sampled at all heights at step 50 with common parameters $T_\infty = 1$, $\Delta t = 0.000001$. Δy had to be changed to compensate for numerical instability.

if h goes to infinity, we obtain

$$\lim_{h \rightarrow \infty} T_I(h) = T_\infty.$$

We now present a model for the drying process. As time evolves, the particle concentration in the fluid region changes due to evaporation at $y = h$ and deposition of particles on the membrane internal structure. Here, we assume there is no effective flow in the fluid region during the drying process, therefore the particle concentration in the fluid region follows a reaction-dispersion equation,

$$\begin{cases} \frac{\partial(\phi C)}{\partial t} = D \frac{\partial^2(\phi C)}{\partial z^2} - \gamma f_d(\phi, C) \\ \frac{\partial \phi}{\partial t} = -\alpha f_d(\phi, C) \end{cases} \quad (4.11)$$

with boundary conditions

$$\begin{cases} \frac{\partial(\phi C)}{\partial z} = -\omega E \phi C, & z = h \\ \frac{\partial(\phi C)}{\partial z} = 0, & z = 0 \end{cases} \quad (4.12)$$

where $0 < z < h(t)$, f_d is the deposition function for the drying process, f_d depends on the porosity and local particle concentration and models how particles are deposited locally within the membrane. ϕ is the porosity, C is the concentration. Here, we consider a particular f_d .

$$f_d(\phi, C) = \phi^{1/2}(C - C_{sat}).$$

To have a fixed domain, we make the next change of variable

$$y = \frac{z}{h(t)}$$

and using the chain rule, we get the next equations

$$\begin{cases} \frac{\partial(\phi C)}{\partial \tau} - \frac{y}{h} \frac{dh}{d\tau} \frac{\partial(\phi C)}{\partial y} = D \frac{1}{h^2} \frac{\partial^2(\phi C)}{\partial y^2} - \gamma f_d(\phi, C) \\ \frac{\partial \phi}{\partial \tau} - \frac{y}{h} \frac{dh}{d\tau} \frac{\partial \phi}{\partial y} = -\alpha f_d(\phi, C) \end{cases} \quad (4.13)$$

For simplicity of the model, we define $\beta = \phi C$, then the equation to consider is given by

$$\begin{cases} \frac{\partial \beta}{\partial \tau} - \frac{y}{h} \frac{dh}{d\tau} \frac{\partial \beta}{\partial y} = D \frac{1}{h^2} \frac{\partial^2 \beta}{\partial y^2} - \gamma f_d(\phi, \beta) \\ \frac{\partial \phi}{\partial \tau} - \frac{y}{h} \frac{dh}{d\tau} \frac{\partial \phi}{\partial y} = -\alpha f_d(\phi, C) \end{cases} \quad (4.14)$$

with boundary conditions

$$\begin{cases} \frac{\partial \beta}{\partial y} = 0, & y = 0 \\ \frac{1}{h} \frac{\partial \beta}{\partial y} = \omega \beta \frac{(T(1,t) - T_\infty)}{k_0}, & y = 1 \end{cases} \quad (4.15)$$

After implementing the code of our PDE, we show the results of some of these experiments next. To numerically solve the system of equations (4.10)-(4.11), we use an explicit backward Euler method and centered spatial discretization. To discretize the spatial domain, $y \in [0, 1]$, we divide it into M subintervals. The grid points within these intervals are denoted as $y_j = j\Delta y$, where y_0, y_1, \dots, y_N represent specific points on the grid. To differentiate between values at different time steps, we utilize the superscripts “ $j + 1$ ” and “ j ”. These superscripts refer to the matters of new and old times, respectively.

Equations (4.11 and 4.12) with boundary conditions lead to

$$\frac{B_i^{j+1} - B_i^j}{\Delta \tau} - \frac{y}{h} \frac{dh}{d\tau} \frac{B_i^j - B_{i-1}^j}{\Delta y} = \frac{D}{h^2} \frac{B_i - 1^j - 2B_i^j + B_{i+1}^j}{(\Delta y)^2} - \gamma \Phi^{\frac{1}{2}} \left(\frac{B_i^j}{\Phi_i^j} - C_{sat} \right) \quad (4.16)$$

$$\frac{\Phi_i^{j+1} - \Phi_i^j}{\Delta \tau} - \frac{y}{h} \frac{dh}{d\tau} \frac{\Phi_i^j - \Phi_{i-1}^j}{\Delta y} = -\alpha \Phi^{\frac{1}{2}} \left(\frac{B_i^j}{\Phi_i^j} - C_{sat} \right) \quad (4.17)$$

$$\frac{B_i^j - B_{i-1}^j}{2\Delta y} = 0 \quad (4.18)$$

$$\frac{B_{i+1}^j - B_{i-1}^j}{2\Delta y} = hw B_i^j \frac{(T(1,t) - T_\infty)}{k_0} \quad (4.19)$$

We solve the following equations iteratively for β and ϕ within a region characterized by moving boundaries $h(t)$. The values of h and $\frac{dh}{dt}$ used in the equation (4.5) and (4.6) for the drying process in Case I are updated in each iteration. Once we obtain the values of ϕ and β , we calculate concentration C using the equation $C = \beta/\phi$.

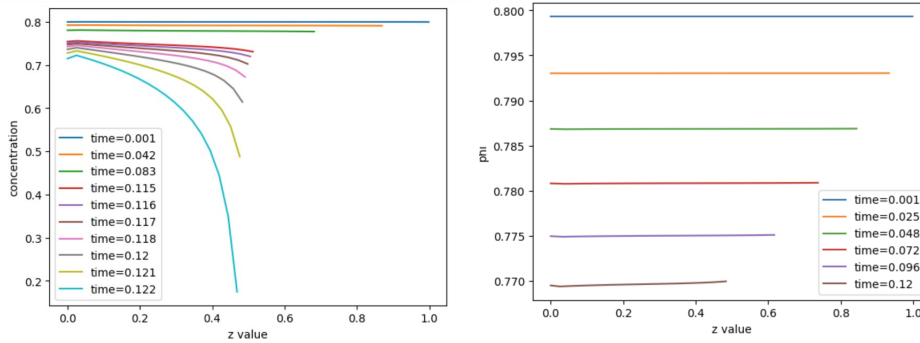


Figure 14. Plot showing the concentration (C) and porosity ϕ in space at different times with the parameters γ_1 , $\omega = 0.10$, $D = 1$ and $C_{sat} = 0.5$.

Figure 14 (a) illustrates the porosity at different time points. Assuming a uniform initial porosity of 0.8, the porosity gradually increases over time. Notably, the porosity significantly increases as we approach the interface. Similarly, in Figure 14 (b), we present the concentration at different time points. Assuming a uniform initial concentration of 0.8, the concentration profile decreases as time progresses. In particular, the concentration decrease is more rapid when nearing the interface.

Also, we numerically investigated the effects of the different parameters on the drying dynamics. This analysis involved varying parameters such as pore geometry, temperature field, and initial particle concentration in assessing their influence on the evaporation rate and particle deposition. The sensitivity analysis results provided insight into the key factors affecting the drying process.

5 Conclusions and Discussions

To summarize, mathematical modeling of drying processes in porous media provides a helpful tool for comprehending and improving drying operations. These models offer valuable insights into drying dynamics and enable designing of effective and sustainable drying processes in various industrial applications by considering the underlying physical and transport phenomena.

While introducing temperature to the filter modeling problem answers some questions, it raises many more. In the macroscopic case, we note that previous efforts [4] have considered the issue in which the evaporation boundary is nonlinear and dependent on particle concentration and porosity. It would be interesting to combine the temperature effects with this aforementioned model. We also discarded the reliance on the evaporation term on pressure, another thing that presents future modeling opportunities. We also know the value of integrating multiple evaporation fronts into the model. While we did not connect the microscopic and macroscopic models, this is another avenue for future exploration. We expect that a network-based approach could give valuable insight into the possibility that the interactions between pores and their neighbors give rise to macroscopic changes in drying behaviors.

6 Acknowledgements

We thank Dr. Edwards and Dr. Fok for running the camp and helpful commentary, Dr. Hangjie Ji for coordinating and providing insightful answers to our questions, the University of Delaware for hosting us and SIAM for funding this camp. Special shout out to all the members of this group that made this a success; you guys rock.

References

- [1] Jacob Bear and M Yavuz Corapcioglu. *Transport processes in porous media*, volume 202. Springer Science & Business Media, 2012.
- [2] Derek B Ingham and Ioan Pop. *Transport phenomena in porous media*. Elsevier, 1998.
- [3] Hangjie Ji and Pejman Sanaei. Mathematical model for filtration and drying in filter membranes. *Physical Review Fluids*, To appear, 2023.
- [4] Pejman Sanaei, Chris Breward, Meredith Ellis, Saem Han, Benjamin Holzer, Hangjie Ji, Hamad El Kahza, Stefan Llewelyn Smith, Shima Parsa, Harry Reynolds, and et al. Evaporation and deposition in porous media. *Mathematics in Industry Reports*, 2022.